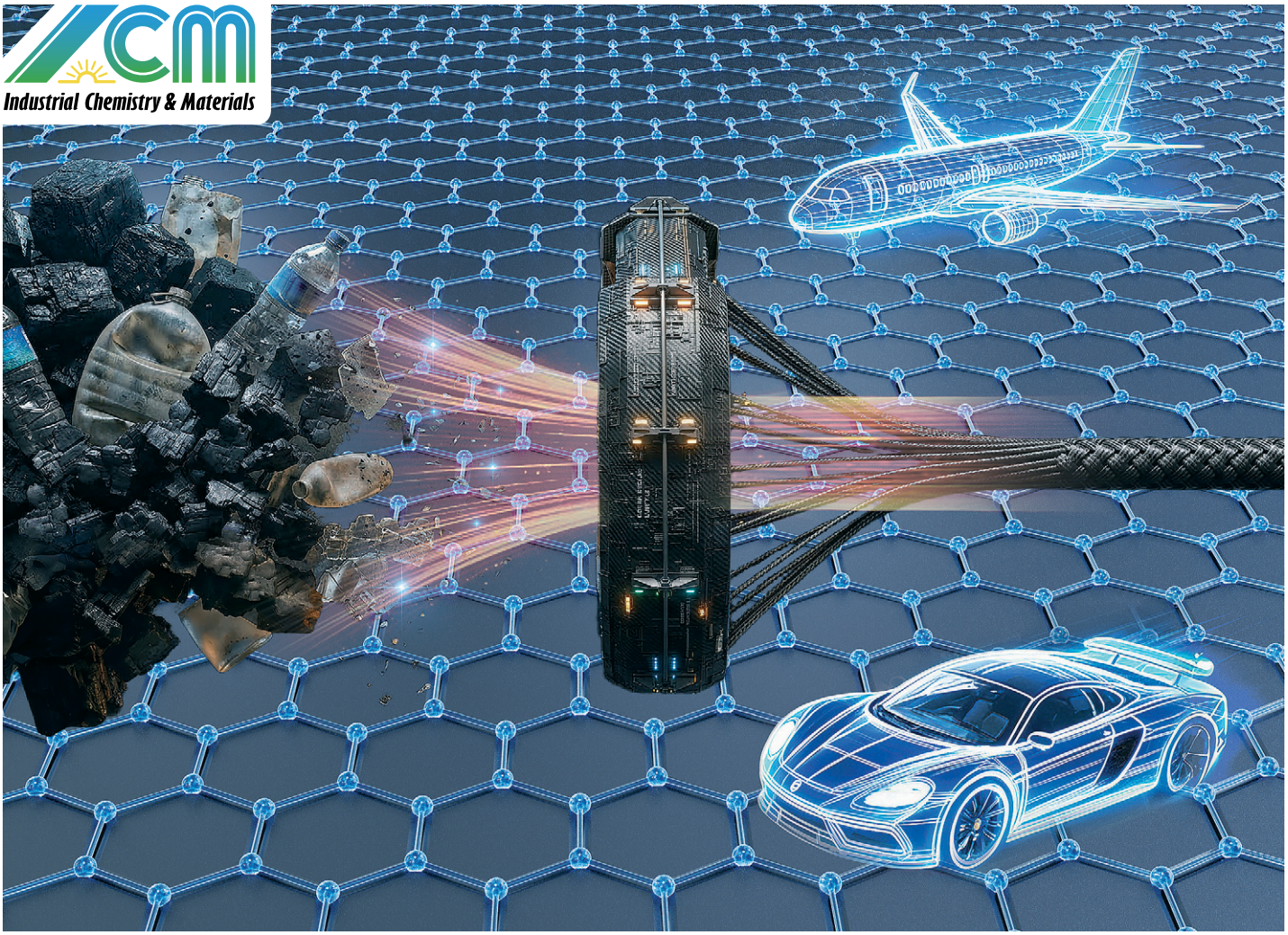

Showcasing research from Maohong Fan's lab at the University of Wyoming and Eric Eddings's lab at the University of Utah.

High-performance carbon fibers fabricated from coal and waste plastics

Plastics are used to produce a solvent which liquefies coal. The liquefied coal is then upgraded and fabricated into high-performance carbon fibers, demonstrating a novel and sustainable valorization pathway for waste plastics and coals.

Image reproduced by permission of Maohong Fan, *Ind. Chem. Mater.*, 2026, **4**, 184.

As featured in:

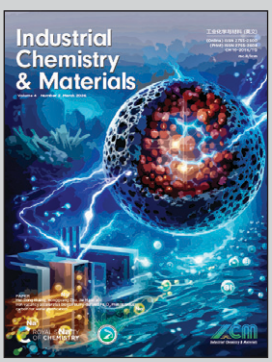

See Eric G. Eddings, Maohong Fan *et al.*, *Ind. Chem. Mater.*, 2026, **4**, 184.

ROYAL SOCIETY OF CHEMISTRY

Industrial Chemistry & Materials

ROYAL SOCIETY OF CHEMISTRY

PAPER

View Article Online
View Journal | View Issue

Open Access Article. Published on 03 October 2025. Downloaded on 5/6/2026 3:37:47 PM.
This article is licensed under a Creative Commons Attribution 3.0 Unported Licence.

Check for updates

Cite this: *Ind. Chem. Mater.*, 2026, **4**, 184

High-performance carbon fibers fabricated from coal and waste plastics

Zhe Chen,[a] Wenjia Wang,[b] Tongtong Wang,[c] Sean Tang,[a] Sabin Gautam,[d] Nilay Saha,[e] Piumi Samarawickrama,[d] So Tie Tjeng,[c] Eric G. Eddings *[b] and Maohong Fan *[fg]

Carbon fibers (CFs) are valuable in applications such as aircraft, automobiles, wind turbines, and energy storage devices. However, the production cost of CFs is high due to the use of conventional precursor polyacrylonitrile, and an affordable substitute is imperative. For the first time, this work combined cheap coal and waste plastic material to fabricate CFs. Currently, conventional disposal methods for waste plastics lack sustainability and profitability. Despite its unpopularity as an energy source, coal can serve as a feedstock for chemicals and materials. High-density polyethylene (HDPE), a commonly used plastic, was hydrogenolyzed into a plastic-derived liquid (PDL). PDL served as an effective solvent during mild solvolysis liquefaction of coal, and the acquired coal–plastic liquid was modified into mesophase coal–plastic liquids (MCPLs). MCPLs were melt-spun and heat-treated into CFs through different heat treatment conditions. The diameters of the CFs were 8.2–45.8 μm, and the Young's modulus and tensile strength were 75–759 GPa and 0.54–4.03 GPa, respectively. The CFs belong to the categories of general-purpose and high-performance CFs. The high-performance CFs (diameter: 8.2 μm, Young's modulus: 759 GPa, and tensile strength: 4.03 GPa) are comparable to commercial and laboratory CFs whose precursors are coal–tar pitch featuring low coal-to-pitch yield, or coal liquefied by conventional, costly solvents. Analysis shows the PDL enhances hydrogen transfer, stabilizes radicals, and promotes mesophase development during thermal treatment. The mechanisms valorizing coal and plastics simultaneously to high-performance CFs are proposed. This work demonstrates a novel and sustainable valorization pathway for waste plastics and coals. Future work will explore industrial-scale plant design, techno-economic analysis, and life-cycle assessment to quantify the economic and environmental impacts.

Received 22nd June 2025,
Accepted 28th September 2025

DOI: 10.1039/d5im00110b

rsc.li/icm

Keywords: Environmentally unfriendly polyacrylonitrile; Valorization of waste plastic and coal; Low CO_2-emission; High-performance carbon fiber.

1 Introduction

Carbon fibers (CFs) are advanced materials that feature lightweight properties and excellent chemical properties.[1,2] CFs are used in automobiles, aircraft, wind turbines, and energy storage devices. However, the high cost is a drawback. The costs of conventional materials such as steel and aluminum are \$0.3–0.5 per kg,[3] and \$1.5–3.5 per kg,[4] respectively. The precursor of most CFs is polyacrylonitrile (PAN), comprising 96% of the CF market volume.[5] For a plant capacity of 3750 t per year, the production cost of PAN-based CF is \$18–30 per kg.[6,7] PAN costs \$1.40–3.60 per t,[2,8] and the as-spun fresh CFs cost \$11.11 per kg, accounting for half of the production cost.[9] Due to the low carbon content of PAN, the yield from fresh CFs to CFs is only 50–55%.[10]

Fortunately, liquefied coal emerged as a viable low-cost CF precursor. Liquefied coal has an approximately 85% yield from fresh CFs to CFs due to its high carbon content, which is the primary reason for its lower production cost.[6,7,10] Its high content of polyaromatic hydrocarbons (PAHs) promotes the formation of graphitic structures during heat treatment. Additionally, melt-spinning of liquefied coal is a more economical and faster technique than solution spinning of PAN.[11] Coal can be liquefied by pyrolysis; the liquid product,

[a] Department of Energy & Petroleum Engineering, University of Wyoming, Laramie, WY 82071, USA
[b] Department of Chemical Engineering, University of Utah, Salt Lake City, UT 84112, USA. E-mail: eric.eddings@chemeng.utah.edu
[c] Department of Chemical and Biomedical Engineering, University of Wyoming, Laramie, WY 82071, USA
[d] Department of Physics and Astronomy, University of Wyoming, Laramie, WY 82071, USA
[e] Department of Chemistry, University of Wyoming, Laramie, WY 82071, USA
[f] College of Engineering and Physical Sciences, and School of Energy Resources, University of Wyoming, Laramie, WY 82071, USA. E-mail: mfan@uwyo.edu
[g] College of Engineering, Georgia Institute of Technology, Atlanta, GA 30332, USA

© 2026 The Author(s). Co-published by the Institute of Process Engineering, Chinese Academy of Sciences and the Royal Society of Chemistry

Open Access Article. Published on 03 October 2025. Downloaded on 5/6/2026 3:37:47 PM.
This article is licensed under a Creative Commons Attribution 3.0 Unported Licence.

called coal tar, is the precursor of general-purpose CFs. By further pyrolysis, coal tar can be modified into coal tar pitch, a mesophase precursor of high-performance carbon fibers (CFs).[12–14] The yield of coal tar from coal pyrolysis is only between 5% and 25%,[15,16] with metallurgical coke being the main product. Another technique, called direct coal liquefaction, can achieve a liquid yield of up to 90%.[17] The method is dissolving the coal and heating it under H_2. However, direct coal liquefaction requires catalysts, temperatures up to 450 °C, and H_2 pressures up to 20 MPa.[18] To tackle these issues, mild solvolysis liquefaction is utilized. It features lower temperature and lower H_2 pressure, no catalysts,[19,20] and lower capital cost. Mild solvolysis liquefaction also avoids excessive cracking,[19,20] reducing the yield of volatiles. A techno-economic analysis showed that with direct coal liquefaction and mild solvolysis liquefaction-generated precursors, CFs cost \$9.5–10.63 per kg,[6,7] only half that of PAN-based CFs.

Like direct coal liquefaction, mild solvolysis liquefaction involves four steps: 1) slurry (coal and solvent mixture) preparation, 2) liquefaction, 3) separation, and 4) solvent recycling.[21] Step 2 is hydrogenation, which heats the slurry under an H_2 atmosphere. Step 3 involves refining, distillation, extraction, and other processes to separate the products. Step 4 recovers the solvent for reuse in step 1. The solvent not only diffuses coal molecules but also donates and shuttles hydrogen. Pure solvents, such as tetralin and anthracene, are used in academic research. Industrial solvents are typically middle or heavy liquefaction products from step 3, containing 2–4 ring PAHs, hydro-PAHs, and paraffins.[21,22] Donor solvents like tetralin have a hydrogen bound to an α carbon (H_α), a naphthenic or aliphatic carbon adjacent to an aromatic ring. These H_α represent a primary hydrogen source. PAHs only have aromatic hydrogen (H_{ar}),[23,24] and are less effective donors. Numerous researchers have liquefied coal by mild solvolysis liquefaction and fabricated CFs.[25–29] Their mechanical performance varies significantly due to differences in feedstock and fabrication conditions. The Young's modulus ranged from 30 to 800 GPa, and tensile strength ranged from 0.9 to 4 GPa, comparable to commercial Mitsubishi and Nippon products.[30,31] The disadvantage of mild solvolysis liquefaction is that to make the slurry pumpable, the solvent–coal mass ratio is typically 1–3,[32,33] and over half of the mild solvolysis liquefaction products are recycled instead of valorized.

This inefficiency can be overcome by introducing a low-cost solvent that does not require recycling. Plastic-derived liquid (PDL), a byproduct of plastic decomposition, is a promising candidate. After mild solvolysis liquefaction, the recovered PDL can be used as consumer products or feedstocks in other processes. Recycling is not necessary due to the vast supply of waste plastics and the added value of the PDL. There has been significant growth in the production of plastics and the generation of waste plastics. In 1950, the world produced only 2 million tons (mt) of plastics, reaching 460 mt in 2019.[34] From 1950 to 2015, 6.3 billion tons (bt) of waste plastics had been generated.[35] By 2035, the cumulative weight of waste plastics would be equal to the fish in the ocean.[35,36] The current disposal methods lack sustainability. Mechanically recycled plastics often deteriorate in quality; landfills, incineration, and mismanagement can release contaminants.[37,38] Combustion of plastics, like coal, emits CO_2, whose capture[39] and utilization[40] entail high costs. One approach to addressing these issues is to upgrade plastics into value-added products through various methods that break down plastic molecules into hydrogen (H_2), monomers, oils, and waxes, which can be used as fuels or chemicals.[38,41–45] PDL contains aliphatics and aromatics, and its similarity to mild solvolysis liquefaction solvent makes PDL a potential solvent. The high hydrogen content of plastics can be inherited by PDL, which reduces the cost of H_2. The above solvent–coal mass ratio is feasible given the low price of waste plastics, ranging from \$0.04 to \$0.34 per kg.[46] So far, few researchers have adopted PDL as a mild solvolysis liquefaction solvent.[47] More publications, including those co-liquefying plastic–coal mixtures,[48–50] utilized solvents that need recycling in a commercial process.

Although 1) PDL has the potential to function as a non-recycling mild solvolysis liquefaction solvent and 2) coal can be liquefied by mild solvolysis liquefaction and fabricated into CFs, no researchers have integrated both. According to the studies[6,7] mentioned above and the economic feasibility of plastic waste, combining 1) and 2) presents a potential cost-effective process to produce CFs. Although a detailed techno-economic analysis is required to prove cost-effectiveness, this work demonstrates technical feasibility, the process is shown in Fig. 1. High-density polyethylene (HDPE) was hydrogenolyzed into a PDL, successfully serving as a mild solvolysis liquefaction solvent to liquefy an Utah low-bituminous coal into a coal–plastic liquid. Our mild solvolysis liquefaction process was conducted at 400 °C and an initial H_2 pressure of 6 MPa. Compared to direct coal liquefaction, a significantly lower pressure allows thinner walls of reactors and tubing. A lower temperature reduces energy consumption, and the absence of catalysts also simplifies the reactor and operation. All these significantly reduce the cost of direct coal liquefaction. A coal–plastic liquid was upgraded into several mesophase coal–plastic liquids (MCPLs) under different upgrading conditions. These MCPLs were fabricated into CFs, and the diameters of CFs ranged from 8.2 to 45.8 μm. The Young's modulus was between 75 and 759 GPa, and the tensile strength was between 0.54 and 4.03 GPa. The CFs qualified as general-purpose CF and high-performance CF, comparable to those of CFs in publications that used pure solvents, as well as commercial CFs. This work establishes a scalable method to convert waste plastics and low-rank coal into carbon fibers by integrating plastic-derived liquids as hydrogen-rich solvents in mild solvolysis liquefaction. We identified a new approach to eliminate waste plastic pollution and valorize inexpensive coal and plastic feedstocks into value-

© 2026 The Author(s). Co-published by the Institute of Process Engineering, Chinese Academy of Sciences and the Royal Society of Chemistry

Open Access Article. Published on 03 October 2025. Downloaded on 5/6/2026 3:37:47 PM.
This article is licensed under a Creative Commons Attribution 3.0 Unported Licence.

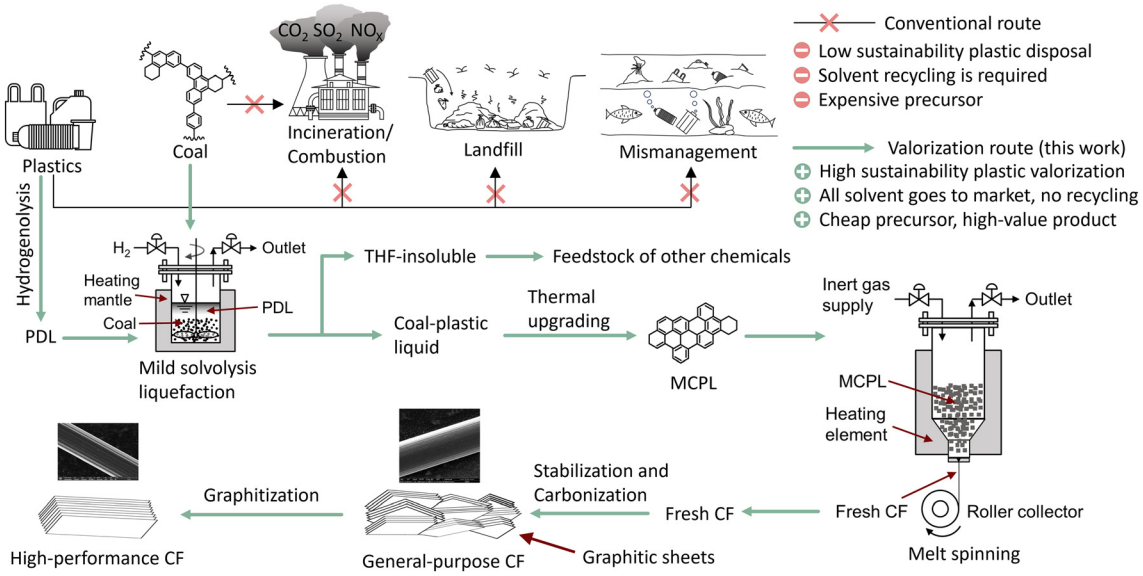

Fig. 1 The process valorizing plastics and coal into carbon fibers.

added CFs. This research has significant implications for environmental sustainability.

2 Results and discussion

2.1 MCPLs

Our mild solvolysis liquefaction used Utah Sufco coal, a low-rank bituminous coal. The proximate and ultimate analyses of this coal are shown in Table S1. In HDPE hydrogenolysis, the yield from HDPE to PDL was 21.5 ± 3.3%. The 1H-NMR results of PDL are shown in Table S2. In our mild solvolysis liquefaction, the weight ratio of coal-to-PDL was 1 : 1. This ratio was selected to simulate industrial process whose ratios are from 1 : 1 to 1 : 3, and also because this ratio was proven effective in our previous work.[51] Higher ratios (*e.g.*, 1 : 0.5) increase viscosity, complicating handling, while lower ratios (*e.g.*, 1 : 5) waste energy on excess solvent heating. Therefore, in this work other ratios were not tested, allowing a full focus on subsequent carbon fiber fabrication. From coal to liquid, tetralin and PDL led to yield of 63.4 ± 0.9% and 62.1 ± 4.3% respectively. This confirms that PDL matches tetralin in liquefaction efficiency, leading to more liquid than coal pyrolysis. MCPLs were prepared by heat-treating coal–plastic liquid under N_2 (essentially a pyrolysis) at different temperatures and soaking times. The weight change during stabilization of fresh CFs was simulated by TGA using MCPLs, and the results are shown in Fig. 2. The change in weight as the temperature rises can indicate oxidation reactions. At ~150 °C, all samples exhibited mass gain due to oxygen intake. Maximum weight occurred between 300 and 340 °C, followed by combustion. Complete weight loss by 550 °C confirms zero ash content. TGA curves will help identify the optimal stabilization temperature in section 2.3.

The upgrading conditions and properties of MCPLs is summarized in Table 1. From MCPL1 to MCPL3, the yield of MCPLs decreased because thermal upgrading vaporized light components. The softening point, quinoline insolubility, and mesophase content increased due to polymerization[52] and the stacking of molecules. The trends of these properties were consistent with upgrading conditions shown in Table 1, suggesting the changes were due to increasing thermal severity. MCTL (mesophase coal–tetralin liquid) was prepared using the same method as coal–plastic liquid, but with tetralin as the solvent instead of PDL. It was then thermally upgraded under the same conditions as MCPL3 for comparison. MCTL's softening point exceeded 350 °C, above melt-spinning limits, and it also features higher quinoline insolubility and lower mesophase content than MCPL3. Spinnable coal or petroleum-derived precursors require a softening point between 230–280 °C,[53] low quinoline insoluble, no ash, and a narrow molecular weight distribution.[53,54] PDL exhibited more favorable melt-spinning properties than tetralin, which can be attributed to the

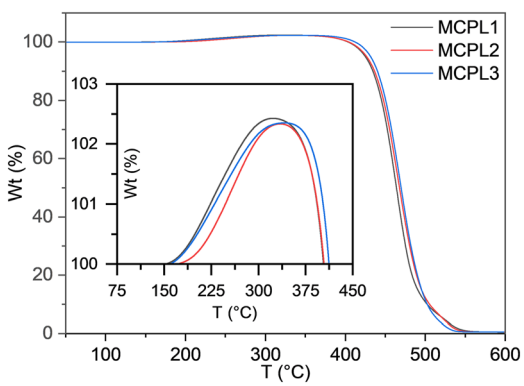

Fig. 2 TGA curves of MCPL1–3. Inset: Detail from 100–450 °C (method: under airflow, ramped at 0.5 °C min^{-1} from room temperature to 600 °C, and held at 600 °C for 2 h).

© 2026 The Author(s). Co-published by the Institute of Process Engineering, Chinese Academy of Sciences and the Royal Society of Chemistry

Open Access Article. Published on 03 October 2025. Downloaded on 5/6/2026 3:37:47 PM.
This article is licensed under a Creative Commons Attribution 3.0 Unported Licence.

Table 1 MCPL upgrading conditions, properties, and melt-spinning parameters

MCPL	Condition	Yield	SP (°C)	QI	MP	Ash	d_o (mm)	T (°C)	P (kPa)	v (m min^{-1})
MCPL1	380 °C, 6 h	28.5%	238	32%	0%	0	0.2	350	452	134
MCPL2	410 °C, 3 h	25.1%	289	48%	42%	0	0.2	390	118	267
MCPL3	425 °C, 3 h	22.7%	302	63%	85%	0	0.3	360	601	267
MCTL	425 °C, 3 h	31.9%	>350	79%	79%	0	—	—	—	—

Yield = (wt of MCPL)/(wt of coal–plastic liquid) × 100%, cited from Wang, *et al.*,[51] the yield of MCPL1 was acquired from communication with Dr. Wang. For MCTL, yield = (wt of MCTL)/(wt of coal–tetralin liquid) × 100%. Condition: the temperature and soaking time when thermally upgrading coal–plastic liquid to MCPL. SP: softening point; QI: quinoline insoluble; MP: mesophase content. Detailed method for measuring these values can be found in the SI. d_o: orifice diameter of the spinneret; T: spinning temperature; p: extrusion pressure over standard atmosphere (101 kPa); v: linear velocity of drum collector.

distribution of functional groups in PDL and tetralin, as indicated by ^{1}H NMR (Table S2). To reveal the detailed mechanisms, more experiments are needed, which is not the scope of this work.

Molecular weight distribution was indicated by the distribution of mass-to-charge ratio (m/z). The results are presented as MALDI-TOF/TOF spectra shown in Fig. 3. MCPLs can be divided based on mass-to-charge ratio (m/z) as monomers (<388 Da), dimers (388–645 Da), trimers (645–890 Da), and tetramers (890–1120 Da).[55,56] From MCPL1 to MCPL3, the tails of MALDI-TOF-MS spectra are more obvious, and the singular peak at 243 Da disappeared on MCPL3. This suggested that small molecules disappeared and larger molecules emerged as the upgrading gained thermal severity. From the lowest recorded m/z (40 Da) to 1120 Da, the average m/z of MCPL1, MCPL2, and MCPL3 are 636, 643 and 650 Da, respectively. Their polydispersity indices were 1.14, 1.13, and 1.12, showing a similar distribution breadth. From MCPL1 to MCPL3, the trend of average m/z is consistent with that of softening point, quinoline insoluble, and mesophase content shown in Table 1. More thorough upgrading led to the polymerization of aromatics in the coal–plastic liquid, thereby increasing the molecular weight of MCPLs, as indicated by the average m/z value. The spinning parameters of the MCPLs are summarized in Table 1. The parameters of a MCPL were determined by trial and error to produce the smallest fresh CFs while maintaining continuous winding. Among the three MCPLs, MCPL2 resulted in the smallest fresh CF at an extrusion pressure of 118 kPa and a collector speed of 267 m min^{-1}. MCPL3 required 601 kPa and a 0.3 mm orifice, indicating a higher viscosity. MCPL1 was spun only at low drum velocity (134 m min^{-1}) to avoid winding discontinuity. Other characterizations of MCPLs can be found in the Supplementary information. The elemental analysis is summarized in Table S3. The XRD pattern and Raman spectra are shown in S1; the extracted crystalline data are presented in Table S4. The polarized light micrographs are shown in S2. The XRD pattern and Raman spectra assist in elucidating the mechanism of heat treatment in section 2.4.

2.2 General purpose CFs

The fresh CFs were stabilized at their MCPL's softening points and carbonized at 1500 °C for a 10 minute soaking

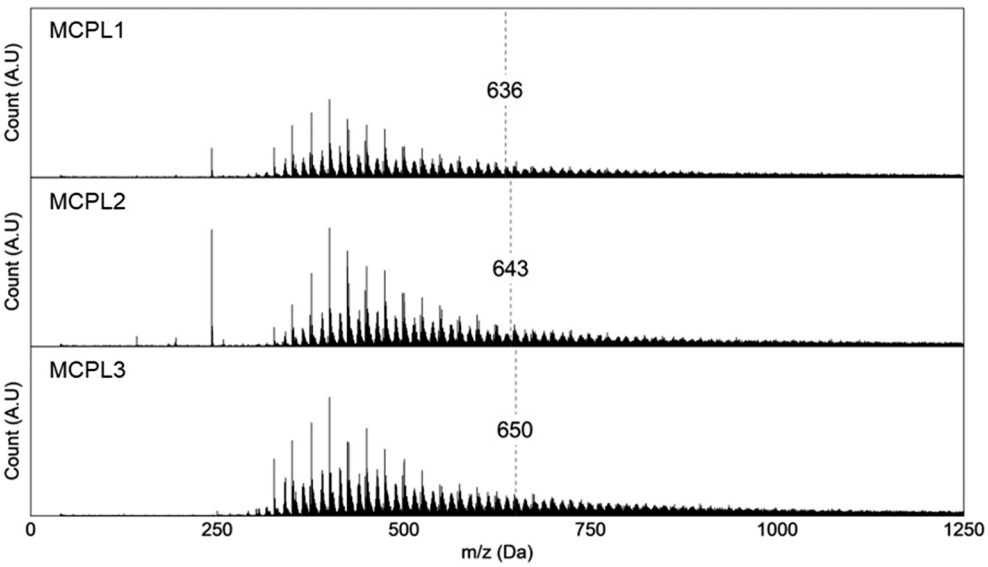

Fig. 3 MALDI-TOF/TOF spectra of MCPLs. The average m/z was indicated by dash lines.

Open Access Article. Published on 03 October 2025. Downloaded on 5/6/2026 3:37:47 PM.
This article is licensed under a Creative Commons Attribution 3.0 Unported Licence.

time. The filaments MCPL1's fresh CFs fused after stabilization. These fresh CFs had large diameters, making it challenging for air to diffuse to the center of the fiber.[57] Therefore, they melted before oxidative cross-linking. Although reducing the ramp rate is a possible solution, it leads to prohibitively long processing times. Ultra-pure oxygen (UHP O_2) was subsequently adopted, and fusing was avoided.

FTIR spectra were acquired to identify changes in functional groups during heat treatment. This information helps reveal the mechanism of heat treatment in section 2.4. The FTIR spectra of MCPLs, fresh CFs stabilized at SPs, and CFs are shown in Fig. 4. MCPLs showed multiple functional groups. The peak at 3040 cm^{-1} is due to C–H stretching vibration on the aromatic rings.[58,59] No peaks were observed at 2955 cm^{-1}; this wavenumber is assigned to stretching and in-plane bending of methyl groups ($-CH_3$).[60] A weak peak at 2922 cm^{-1} corresponded to the asymmetric C–H stretching of methylene groups on the naphthenic ring[61] and the peak at 1440 cm^{-1} was assigned to methylene scissoring bending.[61–63] The 900 and 670 cm^{-1} peaks are assigned to C–H out-of-plane bending of aromatic compounds.[64] The peak at approximately 1587 cm^{-1} was due to the aromatic C═C bond.[58,64] Aromatic and methylene groups were identified, but no methyl groups were found. This result indicates that the methylene groups of fresh CFs belonged to naphthenic rings or bridges between two aromatic rings. After the stabilization of fresh CFs, oxygen-containing functional groups appeared. A plateau between 1436 and 1152 resulted from multiple peaks. The peak at 1253 cm^{-1} was assigned to aryl ethers.[62,65] After stabilization, the peaks centered at 3040, 1439, and between 900 and 700 cm^{-1} exhibit attenuated intensity. Due to the consumption of H,[66–68] the vibration of C–H bonds diminished. The peaks between 1840 and 1650 cm^{-1} were due to the stretching vibration of carbonyl bonds from different functional groups. The tiny peak at 1840 cm^{-1} and the shoulder at 1771 cm^{-1} were assigned to the carboxylic anhydride; the vibrations of the carbonyl bond were attributed to asymmetric and symmetric stretching, respectively.[69] The peak at 1734 cm^{-1} was assigned to a carbonyl bond of an ester.[66] The peaks between 1717 and 1690 cm^{-1} belonged to C═O of aldehyde, carboxyl, and ketone groups.[63] A tiny peak at 1655 cm^{-1}, was due to stretching of quinone C═O.[70] The band at 1300–1000 cm^{-1} was ascribed to the asymmetric stretching vibration of ether and hydroxyl (phenol and alcohol).[67,68] After carbonization, all the above peaks disappeared because the carbonization process eliminated all the functional groups; the up-ramp of the spectrum was due to CFs having higher absorbance at lower wavenumbers.[71]

SEM images of CFs are shown in Fig. 5. Side views show linear streaks parallel to the fiber axis, cross-section views

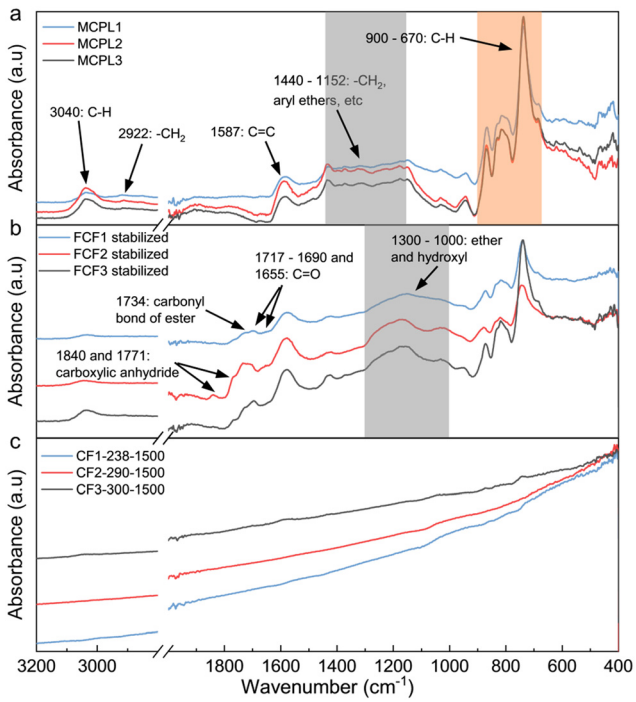

Fig. 4 FTIR spectra of MCPLs, fresh CFs stabilized at SPs, and CFs. In (a), (b) and (c), blue spectra are MCPL1, MCPL2 and MCPL 3, respectively; red spectra are their stabilized fresh CFs; black spectra are CFs, *i.e.*, CF1-238-1500, CF2-289-1500, and CF3-302-1500, respectively.

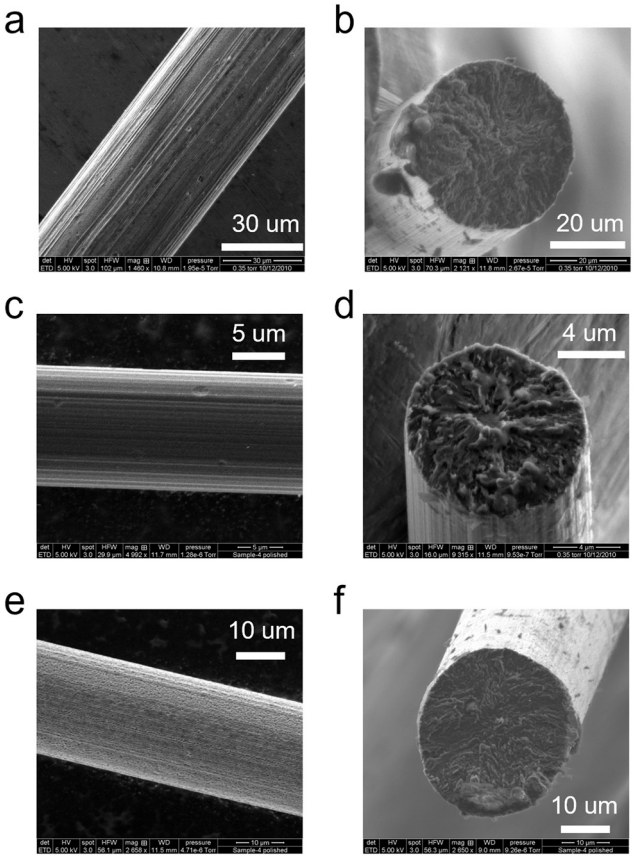

Fig. 5 SEM images of CFs. Column 1: side view, column 2: cross-section view. (a) and (b): CF1-238-1500; (c) and (d): CF2-289-1500; (e) and (f): CF3-302-1500.

© 2026 The Author(s). Co-published by the Institute of Process Engineering, Chinese Academy of Sciences and the Royal Society of Chemistry

Open Access Article. Published on 03 October 2025. Downloaded on 5/6/2026 3:37:47 PM.
This article is licensed under a Creative Commons Attribution 3.0 Unported Licence.

show different arrangements of streaks, CF2-289-1500 had a radial layout, and CF3-302-1500 and CF1-238-1500 had a random layout. These linear structures were edges of carbon sheets, typical of mesophase precursor-based CFs. Due to shear stress,[10,57,72,73] melt-spinning process aligned mesophase molecules parallel to the fiber axis. These molecules became graphitic sheets after heat treatment.

The crystalline data of CFs are shown in Fig. 6a and b. They were determined from the XRD pattern and Raman spectra shown in Fig. S3a and b, and the complete data can be found in Table S5. In the Raman spectrum, theoretical graphite would exhibit a peak at approximately 1586 cm^{-1}, known as the G band, resulting from the E_{2g} vibration mode.[74,75] Therefore, the peaks at 1586 cm^{-1} in the Raman spectra shown in Fig. S3b suggest a graphitic structure. An additional peak is visible at 1344 cm^{-1} in Fig. S3b, referred to as the D band. It has an A_{1g} vibration mode for small crystallites or boundaries of larger crystallites.[74,76] This peak confirms distorted or defective carbon. The presence of G and D bands suggests that the carbon sheets shown in the SEM images (Fig. 5) were graphitic sheets (defective graphene sheets). CF2-289-1500 had the lowest quantity of stacked layers and in-plane crystalline size (12.93 and 5.68 nm), and CF1-238-1500 had the highest (14.81 and 6.64 nm). The diameters and mechanical test results of CFs are shown in Fig. 6c and d, respectively; the detailed data are presented in Table S6. In the following discussion, diameter, Young's modulus, and tensile strength refer to their average values unless specified otherwise. The ranking of diameter is CF2-289-1500 < CF3-302-1500 < CF1-238-1500. Their Young's modulus and tensile strength followed the opposite trend: CF2-289-1500 > CF3-302-1500 > CF1-238-1500. CF2-289-1500 had the smallest diameter, and the highest Young's modulus and tensile strength: 10.8 μm, 194, and 0.85 GPa. However, CF2-289-1500 also had the lowest quantity of stacked layers and in-plane crystalline size, as discussed above. This is because crystalline data does not always align with mechanical properties, as shown in previous works.[20,26,27,77] Section 2.3 will demonstrate that CFs fabricated from the same fresh CFs but with different heat treatments exhibit the same mechanical properties and crystalline data. Crystalline data help reveal the heat treatment mechanism, as discussed in section 2.4. CF2-289-1500 had the smallest diameter and highest stabilization temperature, allowing air to diffuse to the center and a thorough stabilization. CF1-238-1500 had the largest and the lowest stabilization temperature, resulting in insufficient cross-linking. During carbonization, some MCPL molecules slightly migrated or failed to polymerize with surrounding molecules. This undermined the mechanical properties. The spinning parameters and softening points of the MCPLs (Table 1) determined the diameters and stabilization temperatures, respectively,

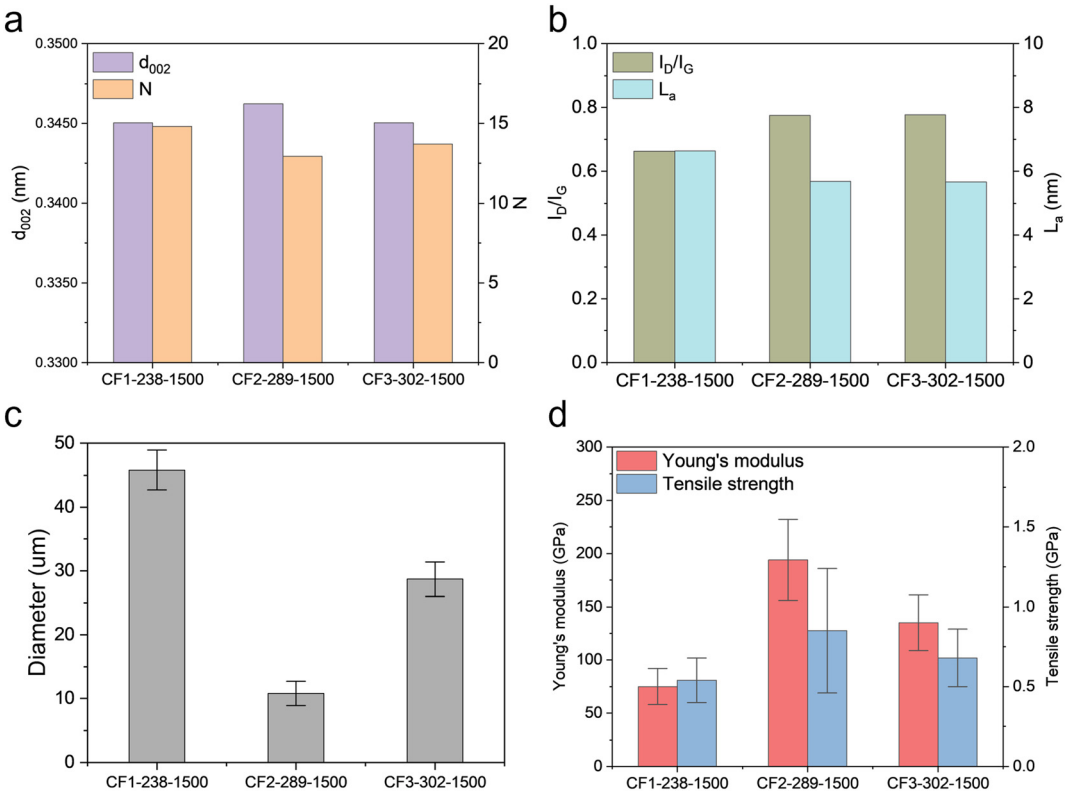

Fig. 6 Crystalline data, diameters, and mechanical properties of CFs fabricated from different MCPLs. (a) d_{002} and quantity of stacked layers (N) extracted from XRD pattern; (b) ratio of I_D to I_G (I_D/I_G) and in-plane crystalline size (L_a) extracted from Raman spectra; (c) diameters of CFs; (d) Young's modulus and tensile strength.

Open Access Article. Published on 03 October 2025. Downloaded on 5/6/2026 3:37:47 PM.
This article is licensed under a Creative Commons Attribution 3.0 Unported Licence.

which influenced the mechanical properties. It was MCPLs that determined the mechanical performances of the CFs.

2.3 High-performance CFs

Fresh CFs of MCPL2 were selected to produce high-performance CFs because CF2-289-1500 had the highest Young's modulus and tensile strength, and the small diameter enables thorough heat treatment. First, the stabilization temperature was optimized. TGA (Fig. 2) and softening point can be used as references. The TGA results show that MCPL2 had the highest weight at 335 °C, and Table 1 indicates its softening point was 289 °C. Therefore, by a 23 °C increment, temperatures of 266, 289, 312, and 335 °C were tested as possible stabilization temperatures. Their TGA weight gains were 1.46%, 1.94%, 2.24%, and 2.33%, respectively. The mechanical performances are shown in Table S6, and the SEM images of CFs are shown in Fig. 7. CF2-312-1500 achieved the highest Young's modulus and tensile strength (201 and 1.11 GPa). Therefore 313 °C was the optimal stabilization temperature. Table S7 shows weight change of CFs during heat treatment. From 266 to 335 °C, weight gain after stabilization dropped monotonically from 10.53% to −17.14%. Weight gain was due to oxygen intake at below 250 °C; weight loss was because cross-linking released H_2O and CO_2 at above 250 °C. 266 °C and 289 °C led to insufficient cross-linking. 335 °C led to excessive cross-linking, and the release of CO, CO_2 and H_2O led to pores, as seen in Fig. 7e. The actual weight stabilization change was different from the TGA results because 1) fresh CFs and MCPL powder had different shapes, and 2) stabilization soaked at a constant temperature while TGA continued ramping. The yield of CFs shown in Table S7 is generally 70–91%, higher than PAN-based CFs.

Next, the soaking time of carbonization was extended from 10 min to 2 h, a "2 h" was added at the end of the label. Finally, graphitization was performed by heating fresh CF to 1500 °C at a rate of 10 °C min^{-1}, soaking for 120 min, and then ramping to 2800 °C at a rate of 5 °C min^{-1}, with a soaking time of 2 h. The resulting product was designated as CF2-312-2800-2h. The SEM images are shown in Fig. 8, although they bear a semblance to the CFs previously shown, crystalline data and mechanical tests indicate that they are different.

The crystalline data of CFs were summarized in Fig. 9a and b. They were obtained from XRD patterns and Raman spectra, as shown in Figs. S3c and d; complete data can be found in Table S5. The quantity of stacked layers and the in-plane crystalline size of CF2-289-1500 was 12.93 and 5.68 nm, slightly lower than CF2-312-1500 (12.97 and 5.75 nm). The quantity of stacked layers and in-plane crystalline size of CF2-312-1500-2h were 20.04 and 6.31 nm, respectively, higher than those of CF2-312-1500. The 2 h carbonization time enabled stacking in the L_c direction and expansion in the L_a direction. The crystalline structure of CF2-313-2800-2h was the closest to graphite. While other CFs' d_{002} and I_D/I_G were above 0.3383 nm and 0.70, CF2-313-2800-2h's dropped to 0.3356 nm and 0.05. Its quantity of stacked layers and in-plane crystalline size were 101.60 and 83.44, which are tremendously higher than those of CF2-312-1500-2h.

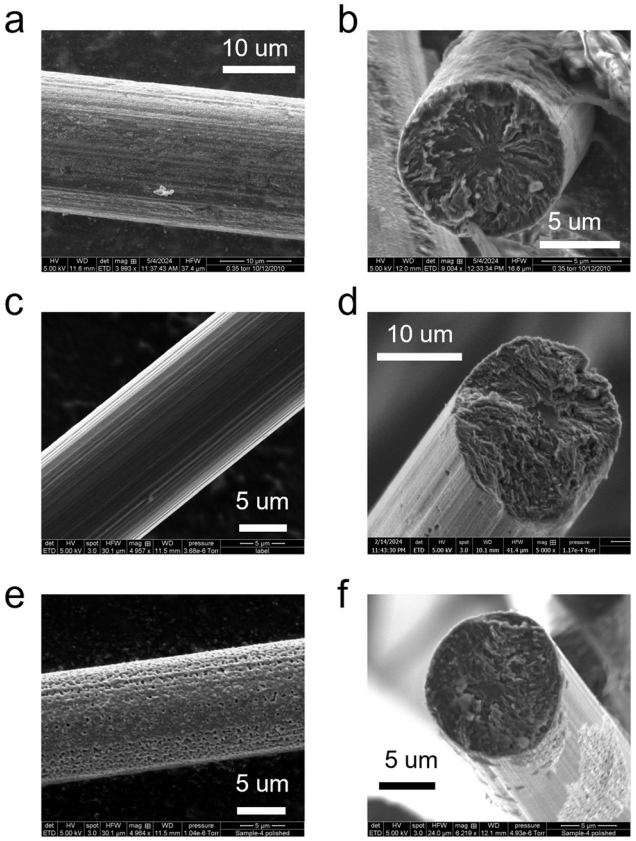

Fig. 7 SEM images of CFs. Column 1: side view, column 2: cross-section view. (a) and (b): CF2-266-1500; (c) and (d): CF2-312-1500; (e) and (f): CF2-335-1500. CF2-289-1500 is shown in Fig. 5c and d.

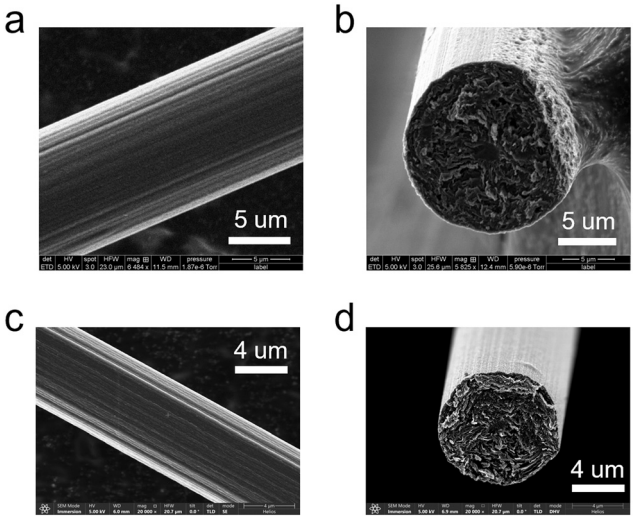

Fig. 8 SEM images of CFs. Column 1: side view, column 2: cross-section view. (a) and (b): CF2-312-1500-2h; (c) and (d): CF2-312-2800-2h.

© 2026 The Author(s). Co-published by the Institute of Process Engineering, Chinese Academy of Sciences and the Royal Society of Chemistry

Open Access Article. Published on 03 October 2025. Downloaded on 5/6/2026 3:37:47 PM.
This article is licensed under a Creative Commons Attribution 3.0 Unported Licence.

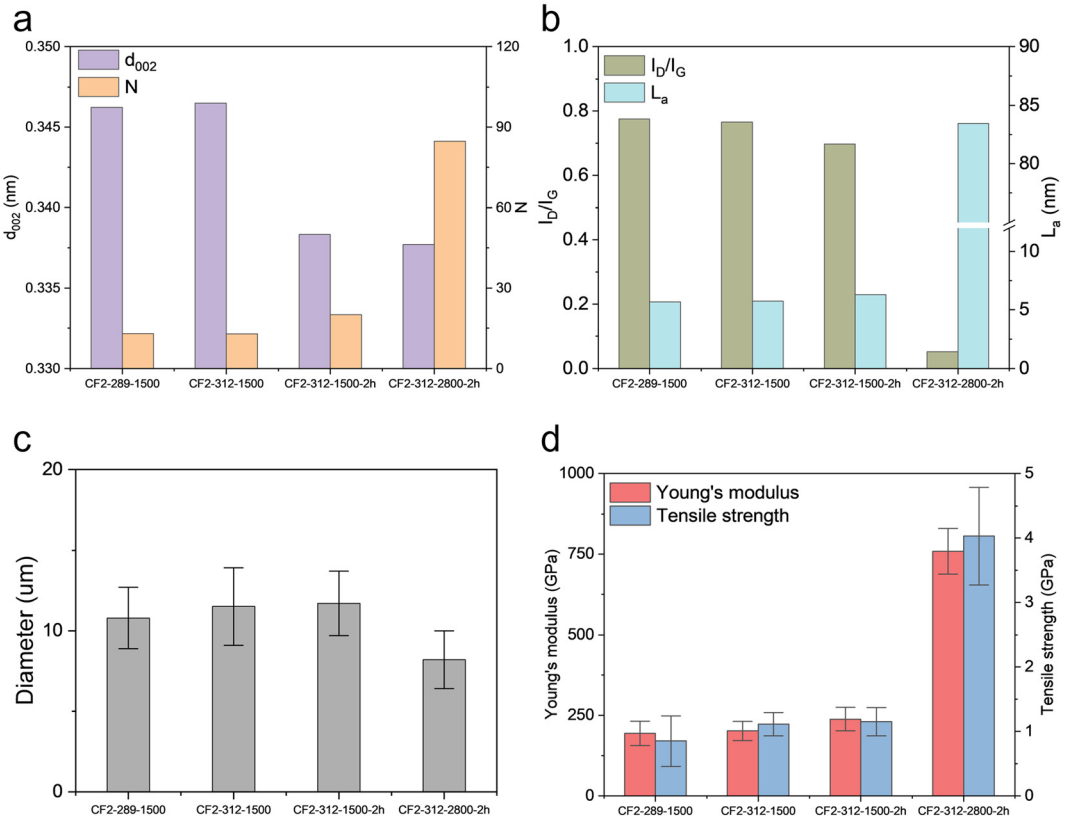

Fig. 9 Crystalline data, diameters, and mechanical properties of different heat-treatment conditions. (a) d_{002} and quantity of stacked layers (N) extracted from XRD pattern; (b) ratio of I_D to I_G (I_D/I_G) and in-plane crystalline size (L_a) extracted from Raman spectra; (c) diameters of CFs; (d) Young's modulus and tensile strength.

Graphitic sheets were stacked in an orderly fashion and expanded with minimal interruption. The diameter, Young's modulus and tensile strength are shown in Fig. 9c and d. In the series of CF2-289-1500, CF2-312-1500, CF2-312-1500-2h, and CF2-312-2800-2h, crystalline data have the same trend with mechanical properties, *i.e.*, the higher the quantity of stacked layers and in-plane crystalline size, the higher the Young's modulus and tensile strength. This suggests that if CFs are fabricated from the same fresh CFs but different heat treatment conditions, the mechanical performance and crystalline data will align. Young's modulus and tensile strength of CF2-312-1500-2h was 238 and 1.15 GPa. Although its tensile strength was almost equal to CF2-312-1500 (1.11 GPa), its Young's modulus was 18.4% higher (201 *vs.* 238 GPa). The Young's modulus and tensile strength of CF2-312-2800-2h reached 759 and 4.03 GPa.

Here, CFs fabricated in this work are classified based on their mechanical performances. In chapter 4 of "New Carbons",[13] Fig. 4-2 shows CFs with Young's modulus of 50–100 GPa, tensile strength of 0.5 to 1.1 GPa are general-purpose CFs. It also states "Carbon fibers with higher strength and modulus than GP-grade (general purpose-grade) are called high-performance grade (HP-grade)". According to Chapter 11 of "Lignin in Polymer Composites",[14] "CFs with high tensile strength (>1.4 GPa) are called 'high-performance carbon fibers'. Relatively low tensile strength CFs are called 'general purpose carbon fibers'.". Therefore, CF2-312-2800-2h is a high-performance CF, and the rest are general-purpose CFs. CF2-312-1500-2h and CF2-312-2800-2h were compared with CFs from other publications and commercial CFs, as shown in Table 2. Compared to other literature, CF2-312-2800-2h had high Young's modulus and tensile strength, and its performance was also comparable to commercial K1392U, K13916, YS-80A, XN-80-60S, and M60J.

2.4 Proposed mechanisms of liquefaction and heat treatment

In this work, mild solvolysis liquefaction was adopted to produce spinnable mesophase-rich precursors. Although numerous studies have been published, no definite reaction mechanisms have been identified for coal hydrogenation.[24,80] A solvent functions to (1) disperse coal macromolecules, (2) enable uniform heat transfer, and (3) donate or transfer hydrogen. Coal obtains hydrogen from the solvent or molecular hydrogen. Solvents are grouped into donors and non-donors. Donors supply hydrogen to coal and regenerate by accepting hydrogen radicals. Donation can proceed *via* a stepwise or concerted mechanism. Coal molecules thermally decompose into radicals. In the stepwise route, hydrogen radicals are thermally cleaved from solvent molecules and bond with coal radicals. The solvent radicals regain new hydrogen radicals and are ready for the next donation

Open Access Article. Published on 03 October 2025. Downloaded on 5/6/2026 3:37:47 PM.
This article is licensed under a Creative Commons Attribution 3.0 Unported Licence.

Table 2 Comparison between CFs of this work, literature-reported CFs, and commercial CFs

Ref.	CF	Precursor	Solvent	ST (°C)	C/G (°C)	*d* (um)	YM (GPa)	TS (GPa)	*ε* (%)
This work	CF2-312-1500-2h	Sufco coal	PDL	313	1500	11.7	238	1.15	0.52
This work	CF2-312-2800-2h	Sufco coal	PDL	313	2800	8.2	759	4.03	0.59
25	MHCTP-420-7	Coal	4H-NP	280	2800	12.0	689	3.09	—
26	CTP-20-GFs-1	Coal	THN	280	2850	10.5	656	3.72	—
	CTP-20-GFs-3	Coal	THN	280	2850	9.6	676	3.49	—
27	C-MP-CFs	Coal	FCC	280	3000	10.3	620	3.86	0.62
	P-MP-CFs	Petroleum	FCC	280	3000	10.0	725	2.89	0.41
	C/P-MP-CFs	CTP : PP = 1 : 1 (mass)	—	280	3000	9.8	773	3.65	0.49
28	H3N3-TLE	GR bitumen coal	MeNP and THN	270	1000	10.2	140	1.80	1.40
	H3N3.5-TLE	GR bitumen coal	MeNP and THN	270	1000	10.5	130	1.80	1.40
	H3N3-TLE	GR bitumen coal	MeNP and THN	270	2800	9.3	450	3.00	0.70
	H3N3.5-TLE	GR bitumen coal	MeNP and THN	270	2800	9.8	370	2.40	0.70
20	DO*-CF	Decant oil	—	300	2000	22.7	795	0.96	0.12
	SFDO-TS	Springfield coal	Decant oil	300	2000	19	479	0.90	0.19
	SFDO-THFS	Springfield coal	Decant oil	300	2000	23.2	475	0.94	0.20
77	CMP-25-GFs	CTP	ETHO	280	3000	12.8	658	3.56	0.54
78	AR50, winding speed 800 RPM	Naphthalene pitch	THF	270	2400	8.0	618	4.00	0.60
79	MPGF-A	Petroleum pitch	—	290	3000	16.9	855	3.09	—
Mitsubishi	K1392U	CTP	—	—	—	—	760	3.70	0.50
Mitsubishi	K13916	CTP	—	—	—	—	760	3.20	0.40
Mitsubishi	K13D2U	CTP	—	—	—	10.0	935	3.70	0.40
Nippon	YS-80A	Pitch	—	—	—	7.0	785	3.63	0.50
Nippon	XN-80-60S	Pitch	—	—	—	10.0	780	3.43	0.50
Toray	M60J	PAN	—	—	—	5.0	588	3.82	0.70

ST: stabilization temperature; C/G: carbonization/graphitization temperature; *d*: diameter; YM: Young's modulus; TS: tensile strength; *ε*: strain-to-failure. CTP: coal tar pitch; PP: petroleum pitch; THN: tetralin; 4HNP: tetrahydronaphthalene; MeNP: methylnaphthalene; FCC: fluid catalytic cracking, no solvents were used. ETHO: ethylene tar hydrodeconstructed oil. K1392U, K13916, and K13D2U: https://mccfc.com/pitch-fiber/, and *ε* was cited from https://www.hajime.com.tw/Upload/product_201805210812374.pdf. YS-80A: https://www.ngfworld.com/dcms_media/other/skill_catalog06-1.pdf. XN-80-60S: https://www.ngfworld.com/dcms_media/other/skill_catalog05.pdf. M60J: https://www.toraycma.com/products/carbon-fiber/.

cycle.[24,81] In the concerted route, a coal radical interacts with a solvent molecule and abstracts a hydrogen radical through a transition state.[82] Typical donor molecules include hydrogenated polycyclic aromatics, such as 1,2,3,4-tetrahydronaphthalene, *i.e.*, tetralin,[83] 9,10-dihydroanthracene,[84] 9,10-dihydrophenanthrene, and 4,5-dihydropyrene.[82] Non-donors may act as hydrogen shuttlers or simply as dispersants; a combination of donor and non-donor may improve liquefaction efficiency.[80,85] Shuttlers like naphthalene, anthracene, and phenanthrene[80] can be hydrogenated by donor or molecular hydrogen to form a derived donor. Paraffins are non-shuttlers, acting as dispersants.[86] The donating ability of a solvent molecule depends on the chemical environments of hydrogen atoms.[23] Hydrogens on saturated carbons adjacent to

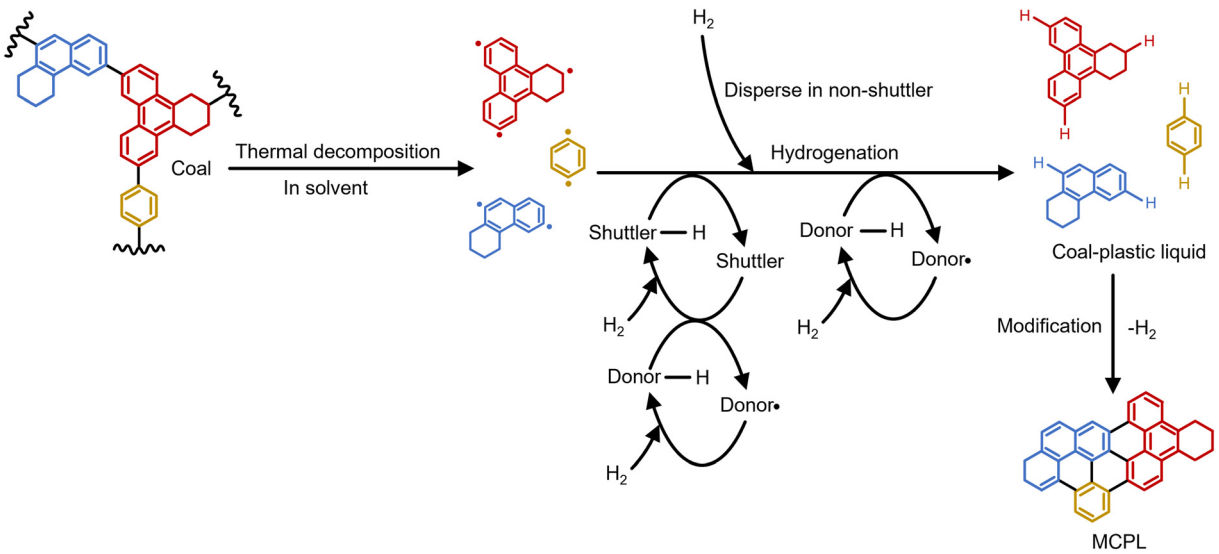

Fig. 10 Proposed mechanisms of mild solvolysis liquefaction.

© 2026 The Author(s). Co-published by the Institute of Process Engineering, Chinese Academy of Sciences and the Royal Society of Chemistry

Open Access Article. Published on 03 October 2025. Downloaded on 5/6/2026 3:37:47 PM.
This article is licensed under a Creative Commons Attribution 3.0 Unported Licence.

aromatic rings (H_α) are the most effective. Aromatic (H_{ar}), methyl (H_γ), and aliphatic methylene hydrogens (H_β) have a weaker donating capability. The 1H-NMR of PDL (Table S2) confirmed the presence of H_{ar} of aromatics, H_α on carbon alpha to aromatic ring, H_γ of methyl group, and H_β of methylene and methylidyne group.[23,51] H_α contributes to donating hydrogen; other hydrogens belong to shuttlers or non-shuttlers. Previous works on HDPE hydrogenolysis[87,88] reported that PDL comprises alkanes, olefins, naphthenes, and aromatics. Thus, our mild solvolysis liquefaction process likely involves multiple hydrogen transfer modes, as shown in Fig. 10. Subsequently, the coal–plastic liquid is thermally upgraded to MCPL through a polymerization process that forms PAHs by dehydrogenation. These sheet-like PAHs subsequently stacked into basic structural units, or mesogens.[89]

Heat treatment includes multiple steps of stabilization and carbonization, and optional graphitization. Without stabilization, fresh CFs fuse during carbonization. Stabilization chemically crosslinks the fresh CFs, making them infusible. As shown in Fig. 4, after stabilization, the peaks of aromatic C–H and methylene groups shrink and disappear, and oxygen-containing groups appear. The mechanism of stabilization is illustrated in Fig. 11. When the temperature is below 250 °C, methylene groups are oxidized into ketone groups, and some studies have also found that aromatic C–H groups are converted into quinone groups.[70] Crosslinking occurred at higher temperatures between 250 and 400 °C. The C–C bond on the naphthenic rings ruptured, and aldehyde, carboxyl, anhydride group, and intramolecular peroxide were formed subsequently.[63] These functional groups on neighboring molecules are crosslinked by losing CO, CO_2, or H_2O, or simply radical recombination. The aromatic rings' surface was oxidized to phenol at this temperature interval.[90] Temperatures above 400 °C produce excessive phenols and rupture aromatic rings by opening C–C bonds, leading to the formation of carboxylic acid.[90] The defects of polyaromatic structures reduce mechanical properties.

Carbonization can be divided into several phases. Drbohlav *et al.*[61] discussed the chemical reactions from a functional group perspective, and Oberlin[89] summarized the mechanisms based on crystalline structures. The FTIR spectra in Fig. 4 show that all the functional groups disappeared after carbonization. As shown in Fig. 12, the crosslinks vaporize as CO, CO_2, and H_2O at between 400 and 600 °C,[61] and C–C bond replaces the crosslinks. At a maximum temperature of 800 °C, all heteroatoms are eliminated.[89] In MCPL, molecules are sheet-like aromatics, and multiple such aromatics are piled up in parallel, forming basic structural units.[89] Melt-spinning loosely aligned these basic structural units parallel to the axis of fresh CFs. The effect of carbonization at 1500 °C is revealed by comparing crystalline data of MCPLs (Table S4) and corresponding CFs (Table S5, or Fig. 6a and b). When MCPL1, MCPL2, and MCPL3 were fabricated into CF1-238-1500, CF2-289-1500, and CF3-302-1500, respectively, the quantity of stacked layers increased by 48.55%, 17.33% and 38.10%, and the in-plane crystalline size increased by 27.45%, 10.29% and 0.71%. The increased percentage of stacked layers was larger than the in-plane crystalline size, suggesting that carbonization facilitated stacking rather than in-plane expansion of graphitic sheets.

Crystalline data also revealed that a longer soaking time benefited stacking and in-plane expansion. In Fig. 9a and b (from Table S5), the quantity of stacked layers and in-plane crystalline size of P4-313-1500-2h are 55.83% and 9.74% higher than P4-313-1500. The limited increase in the amount of stacked layers and in-plane crystalline size led to the development of general-purpose CFs. To produce high-performance CFs, graphitization is necessary at above 1500–2000 °C. The effect of graphitization can also be revealed in Fig. 9a and b (from Table S5). When graphitized at 2800 °C, the quantity of stacked layers and in-plane crystalline size of P4-313-2800-2h reached 101.60 and 83.44 nm, they are 5.07 and 13.22 times of P4-313-1500-2h, respectively. In contrast to carbonization, graphitization has a more pronounced

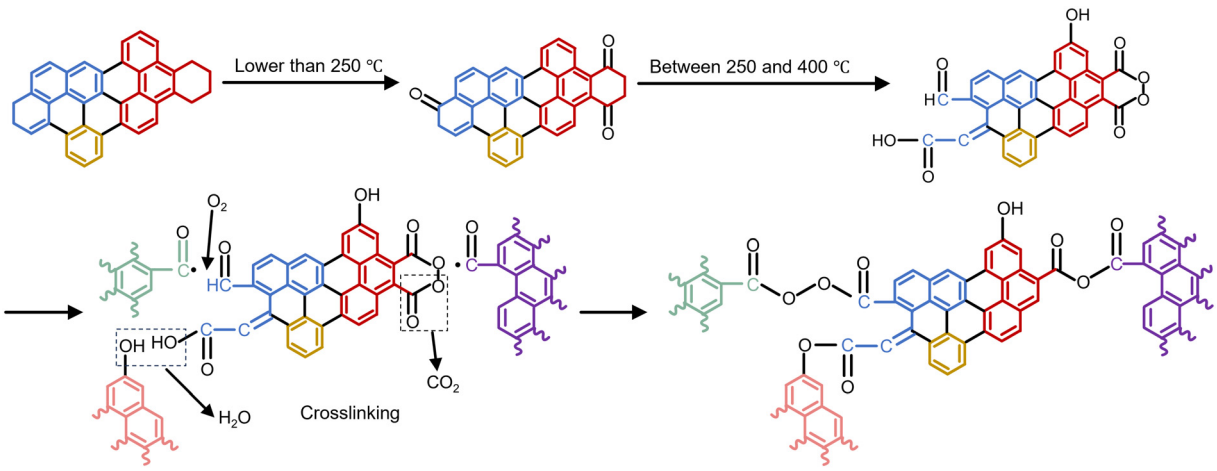

Fig. 11 Proposed mechanism of stabilization when temperature is lower than 250 °C, and between 250 and 400 °C.

Open Access Article. Published on 03 October 2025. Downloaded on 5/6/2026 3:37:47 PM.
This article is licensed under a Creative Commons Attribution 3.0 Unported Licence.

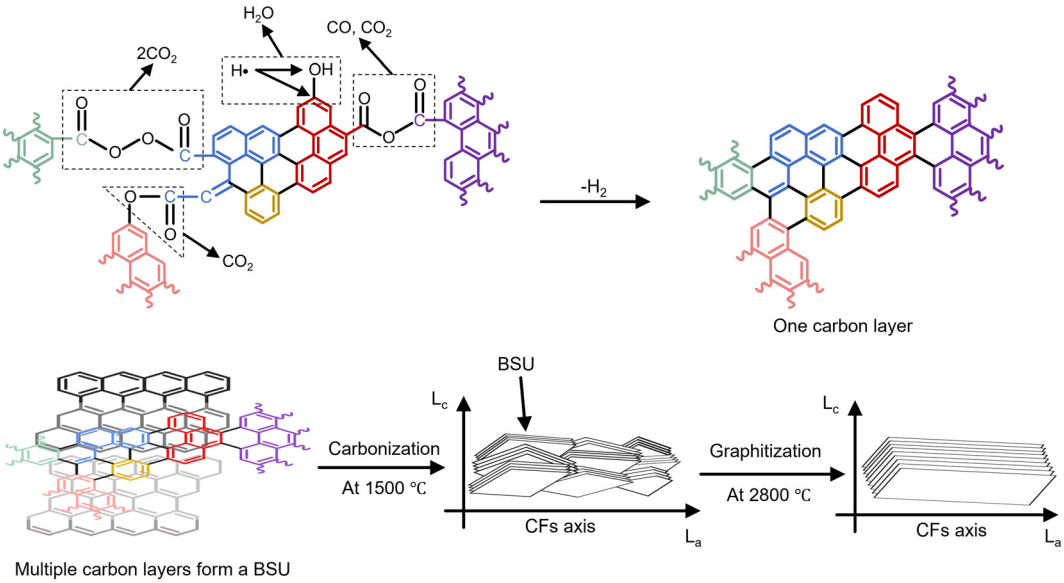

Fig. 12 Proposed mechanisms of carbonization and graphitization. Upper: change of functional groups; lower: change of crystalline structure.

effect on in-plane expansion. At temperatures above 1500 °C, the basic structural units disappeared,[89] graphitic sheets merged into a stack of wrinkled, large ones at approximately 1700 °C. Wrinkles are eliminated between 1900 to 2100 °C, and above 2100 °C, the in-plane defects diminish. The schematic of organized graphitic sheets can be seen in Fig. 12.

2.5 Considerations for industrial implementation

This work demonstrated lab-scale feasibility, and industry-scale implementation will be studied in the next step. This future work includes 1) designing a plant, 2) techno-economic analysis, and 3) life-cycle assessment. Multiple key challenges should be addressed. Continuous mild solvolysis liquefaction requires reactors operating at 400–450 °C and 6 MPa H_2 pressure, capable of handling coal–slurry mixtures with variable rheology. The solvent, *i.e.*, PDL, must remain stable without deleterious contamination. Integrating hydrogenolysis and mild solvolysis liquefaction requires precise control of residence time, heat transfer, and phase separation to manage residual polymers, gases, and solubilized coal. Melt-spinning at temperatures up to 400 °C necessitates viscosity and pressure regulation for stable extrusion and filament collection. Stabilization must ensure uniform oxidative crosslinking to prevent melting during carbonization, while carbonization and graphitization (1500–2800 °C) require energy-efficient furnaces with inert atmospheres. Future work will also optimize the material balance (coal and waste plastics to carbon fiber) and address safety for H_2 and liquefied plastics (*e.g.*, pressure vessel design). These efforts, aligned with the workflow in Fig. 13, will inform techno-economic analysis and life-cycle assessment. Techno-economic analysis investigates the economic impact, including capital cost and long-term cash flows. Life-cycle assessment results quantify environmental sustainability, such as CO_2-equivalent.

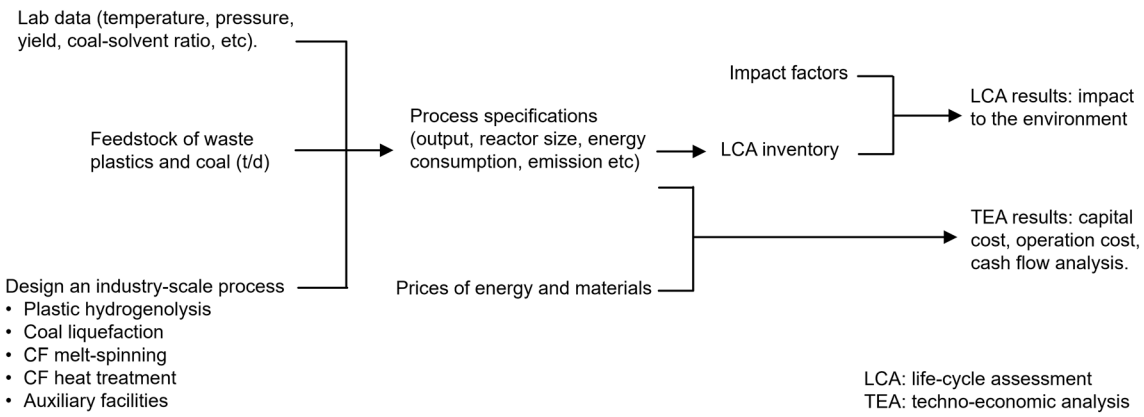

Fig. 13 Method and workflow of techno-economic analysis and life-cycle assessment.

© 2026 The Author(s). Co-published by the Institute of Process Engineering, Chinese Academy of Sciences and the Royal Society of Chemistry

Open Access Article. Published on 03 October 2025. Downloaded on 5/6/2026 3:37:47 PM.
This article is licensed under a Creative Commons Attribution 3.0 Unported Licence.

3 Conclusion

This study demonstrates an integrated process for producing advanced carbon fibers (CFs) from waste high-density polyethylene (HDPE) and coal, offering a sustainable alternative to conventional methods. HDPE was hydrogenolyzed into plastic-derived liquid (PDL), which served as an effective solvent for mild solvolysis liquefaction, producing coal–plastic liquid. This product was upgraded into mesophase coal–plastic liquids (MCPLs), and melt-spun into CFs with diameters of 8.2–45.8 μm, Young's modulus of 75–759 GPa, and tensile strength of 0.54–4.03 GPa, meeting general-purpose or high-performance CF standards. The optimal MCPL (coal–plastic liquid upgraded at 410 °C and 3 h soak) yielded the smallest-diameter CFs with superior mechanical properties. Engineering challenges, including reactor design for mild solvolysis liquefaction, parameter tuning for melt-spinning, and heat treatment conditions, were addressed, establishing lab-scale feasibility. PDL and MCPLs proved potential alternatives to conventional, costly solvents and polyacrylonitrile, respectively. This process valorizes waste plastics and coal, reducing environmental impact while enabling economic gains. Future work will focus on industrial-scale plant design, techno-economic assessment, and life-cycle assessment. The economic impact and environmental sustainability will be quantified.

4 Experimental section

4.1 Preparation of MCPL

PDL, coal–plastic liquid, and MCPL were prepared by HDPE hydrogenolysis, mild solvolysis liquefaction, and thermal upgrading of the coal–plastic liquid, respectively. The detailed procedures can be found in previous work,[51] which is also provided in the SI. These three processes were all performed in batch reactors. HDPE was hydrogenolyzed under an initial H_2 pressure of 6 MPa at 450 °C for 60 min; the tetrahydrofuran (THF)-soluble fraction was separated and is called plastic-derived liquid. Mild solvolysis liquefaction was performed by mixing PDL and Utah Sufco coal at a mass ratio of 1 : 1. The mixture was heated under an initial H_2 pressure of 6 Mpa at 450 °C for 60 min. After mild solvolysis liquefaction, the product, insoluble in hexane but soluble in THF is defined as coal–plastic liquid. To increase the mesophase content, coal–plastic liquid was thermally upgraded under N_2 flow at various temperatures and durations, and the reactor's residual material is referred to as mesophase coal–plastic liquid (MCPL). HDPE hydrogeniolysis, mild-solvolysis liquefaction, and thermal upgrading were repeated three times to make sure repeatability. The characterization data (*e.g.* yield) were averaged.

4.2 Production of carbon fibers

Melt-spinning was carried out using an AT225 melt-spinning machine. The MCPL was ground using a mortar and pestle and then filtered through a 425 μm sieve. The ground MCPL was poured into a feed cylinder on the machine. Helium (He) purged the cylinder, and the pressure maintained ambient. Before spinning, the cylinder was preheated to a setpoint temperature (the spinning temperature) and allowed to soak for 15 minutes. The pressure slowly increased during spinning, and a rotating drum collected the as-spun fresh CFs.

The subsequent heat treatment procedure included stabilization and carbonization to produce general-purpose CF, and an extra graphitization was applied to produce high-performance CF. Stabilization was performed using a Thermo Scientific Lindberg Blue M tube furnace. Under air or oxygen, the temperature ramped at 0.5 °C min^{-1} to a set point (stabilization temperature) and maintained isothermally for 1 h. Carbonization was performed by heating at 10 °C min^{-1} to the final carbonization temperature and soaking. If graphitization was needed, the same carbonization protocol was followed, and after soaking, the furnace ramped at 5 °C min^{-1} to 2800 °C before another soaking. Details on soaking durations are provided in section 2.2 and 2.3. If only carbonization were performed and the soaking time were 10 minutes, a Carbolite HTRH 18/40/500 tube furnace would be used. Otherwise, for longer soaking times or graphitization, an MRF T-4X8-G-G-3000-VM-G high-temperature furnace was utilized. The heat-treated fibers were called carbon fibers (CFs). In this work, a category of CF was denoted as "CF2-289-1500", meaning this CF was produced by spinning MCPL no. 2, stabilized at 290 °C for 1 h, and carbonized at 1500 °C for 10 min. If the CF was graphitized, only the graphitization temperature was shown, if soaking time was not 10 min, the actual time was given in the label. For example, "CF2-312-2800-2h" denoted this CF was graphitized at 2800 °C for 2 h.

4.3 Characterization methods

If not specified, characterization was performed for both MCPLs and CFs. To analyze the protons of PDL, Proton Nuclear Magnetic Resonance (^{1}H NMR) analysis was performed on a 500 MHz ^{1}H NMR spectrometer (AVANCE III HD, Bruker, Billerica, MA, USA). The mesophase contents of MCPLs were determined by polarized light micrographs, acquired by a polarized light microscope (POM, BH200-MR, Ningbo Sunny Instruments Co., Ltd, China). The softening points of MCPLs were measured using a hybrid rheometer/dynamic mechanical analyzer (HR 20, TA Instruments, New Castle, DE) in a nitrogen-purged atmosphere. All three characterization methods above were based on previous work,[51] and the details are also provided in the SI. Fourier Transform Infrared Spectroscopy (FTIR) was conducted using attenuated total reflection (ATR) sampling mode. The FTIR spectra were measured on a ThermoFisher iS50 ATR to analyze the functional groups during heat treatment. The number of scans was 64, the resolution was 4 cm^{-1}, and the

© 2026 The Author(s). Co-published by the Institute of Process Engineering, Chinese Academy of Sciences and the Royal Society of Chemistry

Open Access Article. Published on 03 October 2025. Downloaded on 5/6/2026 3:37:47 PM.
This article is licensed under a Creative Commons Attribution 3.0 Unported Licence.

wavelength ranged from 4000 to 400 cm^{-1}. Thermogravimetric analysis (TGA) of MCPLs was done on a TA Instruments Q600 SDT analyzer. The temperature ramped at 0.5 °C min^{-1} from room temperature to 600 °C and was then held for 2 hours. The atmosphere was 100 mL min^{-1} air. Elemental analysis of MCPLs contained two parts: carbon, nitrogen and sulfur (CNS), and oxygen and hydrogen (OH) elements. CNS were analyzed on a Thermo Scientific Delta V Isotope Ratio Mass Spectrometer (IRMS) in continuous flow mode and connected to Thermo Flash isolink elemental analyzer (EA) *via* a Finnigan ConFlo IV interface. OH was also run on IRMS in the same mode but connected to a high-temperature conversion elemental analyzer (TC/EA) *via* a Conflo IV. The molecular weight distribution of MCPLs was indicated by the distribution of mass-to-charge ratio (m/z). The data were acquired using a Bruker Ultraflex Extreme MALDI-TOF/TOF mass spectrometer (Bruker Daltonics, Bremen, Germany), equipped with a Smartbeam-II Nd:YAG laser (355 nm, with a repetition rate of up to 2 kHz). Analyses were conducted in positive ion mode using reflector detection. MCPL powders were suspended in water. A single drop of the suspension was transferred to a ground stainless steel MALDI plate using a Pasteur pipette, and the solution was dried at room temperature. To study the crystalline structures, X-ray diffraction (XRD), crystallography, and Raman spectroscopy were performed. The XRD patterns were acquired on a Rigaku SmartLab3 X-ray diffractometer, with an X-ray source from a Cu target; the wavelength was 0.154 nm. Before analysis, all samples were ground and passed through a 250 μm sieve. To analyze MCPLs, the diffraction angle (2θ) of the XRD pattern was scanned from 10° to 90°, with a scanning speed of 4° min^{-1}. To analyze the CFs, the XRD pattern was scanned from 20° to 30°, with a scanning speed of 1° min^{-1}. Bragg's law calculated the distance between two adjacent planes (d_{002}); the height of the stacking of these planes, L_c, was calculated by Scherrer's equation.[91] The quantity of stacked layers were denoted by N. Raman spectra were measured on a Horiba confocal Raman microscope; the wavelength of the excitation laser was 532 nm; the D band (~1350 cm^{-1}) and G band (~1580 cm^{-1}) were used to evaluate graphitic disorder. The defects of the material were quantify by the ratio of D band to G band intensities, labeled as I_D/I_G. In-plane crystalline size (L_a) was calculated by eqn (1).[92]

$$L_a = 2.4 \times 10^{-10} \lambda^4 \left(\frac{I_D}{I_G}\right)^{-1}. \quad (1)$$

Here L_a is the in-plane crystalline size (nm), and I_D and I_G are the intensities of D and G bands, respectively (A.U).

To observe the morphology and measure the diameters of CFs, a Quanta 450 FEG scanning electron microscope (SEM), a Thermo Scientific Helios 5 UX Focus Ion Beam/Scanning Electron Microscope (FIB-SEM), and a Leica Microsystems DM2900P microscope were used, depending on availability, to visualize CFs. The mechanical properties of CFs were measured on a HY005E single fiber strength tester. In this work, one fiber from a category of CFs is called a filament. The method was based on the ASTM C1557 standard. The sample mount was prepared by piercing A4 paper with a three-hole punch. A filament was glued by Gorilla super glue and JB Epoxy adhesive across the hole and dried for 24 h. During the mechanical test, the pull speed was 2 mm min^{-1}, at least ten filaments were tested for each category of CFs, and the gauge length of the specimen was 7.5–30 mm. Young's modulus and tensile strength were determined by the stress–strain (σ–ε) curves.

Author contributions

Zhe Chen: conducted all the melt-spinning, mechanical tests, and relevant characterizations and wrote this manuscript. Wenjia Wang: devised the carbon fiber preparation methodology, synthesized coal-plastic liquid using coal and plastic-derived solvent, and performed relevant characterizations. Wang Tongtong: assisted Zhe Chen in conducting melt-spinning work. Sean Tang: operated a high-temperature furnace for graphitization. Sabin Gautam: performed Raman spectroscopy on carbon fibers. Nilay Saha: conducted matrix-assisted laser desorption ionization-time of flight mass spectrometry analysis to get molecular weight distributions. Piumi Samarawickrama: performed Raman spectroscopy on carbon fibers and coal–plastic liquid. Eric Eddings: led the development of coal–plastic liquids preparation technology and supervised Wenjia Wang. Maohong Fan: led the development of carbon fiber production technology and supervised Zhe Chen.

Conflicts of interest

The authors declare no conflict of interest.

Data availability

Supplementary information is available. See DOI: **https://doi.org/10.1039D5IM00110B**.

The data that support the findings of this study are available from the corresponding author upon reasonable request.

Acknowledgements

This work was made possible by funding from the Department of Energy, award number DE-FE0031880.

References

1 H. Khayyam, R. N. Jazar, S. Nunna, G. Golkarnarenji, K. Badii, S. M. Fakhrhoseini, S. Kumar and M. Naebe, PAN precursor fabrication, applications and thermal stabilization process in carbon fiber production: Experimental and mathematical modelling, *Prog. Mater. Sci.*, 2020, **107**, 100575.

© 2026 The Author(s). Co-published by the Institute of Process Engineering, Chinese Academy of Sciences and the Royal Society of Chemistry

Open Access Article. Published on 03 October 2025. Downloaded on 5/6/2026 3:37:47 PM.
This article is licensed under a Creative Commons Attribution 3.0 Unported Licence.

2 A. Jana, T. Zhu, Y. Wang, J. J. Adams, L. T. Kearney, A. K. Naskar, J. C. Grossman and N. Ferralis, Atoms to fibers: Identifying novel processing methods in the synthesis of pitch-based carbon fibers, *Sci. Adv.*, 2022, **8**, eabn1905.
3 What are the 9 operating costs of a steel manufacturing business?, **https://businessplan-templates.com/blogs/running-costs/steel-manufacturing**, (accessed 23 September 2025).
4 A-line corporation, 5 Factors that impact the cost of aluminum extrusions, **https://www.alineautomation.com/5-factors-that-impact-the-cost-of-custom-aluminum-extrusions/**, (accessed 23 September 2025).
5 S. Das, J. Warren, D. West and S. M. Schexnayder, *Global carbon fiber composites supply chain competitiveness analysis*, 2016.
6 S. Das and P. Nagapurkar, *Sustainable coal tar pitch carbon fiber manufacturing*, Oak Ridge, TN (United States), 2021.
7 P. Nagapurkar and E. Lara-Curzio, Technoeconomic and life cycle energy analysis of carbon fiber manufactured from coal via a novel solvent extraction process, *Int. J. Coal Sci. Technol.*, 2025, **12**, 27.
8 imarc, Polyacrylonitrile (PAN) pricing report 2024: price trend, chart, market analysis, news, demand, historical and forecast data, **https://www.imarcgroup.com/polyacrylonitrile-pricing-report**, (accessed 23 September 2024).
9 Procurement Resource, Carbon fibre prices trend and forecast, **https://theprocurementexpert.com/carbon-fibre-prices/**, (accessed 23 September 2025).
10 P. Morgan, *Carbon fibers and their composites*, CRC Press, Boca Raton, 1st edn, 2005.
11 M. Weisenberger, in *(323a) Coal to Carbon Fiber*, AlChE Annual Meeting, Pittsburg, PA, 2018.
12 S.-J. Park, *Carbon fibers*, Springer Nature Singapore Ptd Ltd, 2nd edn, 2018.
13 M. Inagaki, *New carbons - control of structure and functions*, Elsevier, 2000.
14 S. Chatterjee, T. Saito and P. Bhattacharya, in *Lignin in Polymer Composites*, Elsevier, 2016, pp. 207–216.
15 J. Wu, Q. Liu, R. Wang, W. He, L. Shi, X. Guo, Z. Chen, L. Ji and Z. Liu, Coke formation during thermal reaction of tar from pyrolysis of a subbituminous coal, *Fuel Process. Technol.*, 2017, **155**, 68–73.
16 M. D. Casal, M. A. Díez, R. Alvarez and C. Barriocanal, Primary tar of different coking coal ranks, *Int. J. Coal Geol.*, 2008, **76**, 237–242.
17 I. Mochida, O. Okuma and S. H. Yoon, Chemicals from direct coal liquefaction, *Chem. Rev.*, 2014, **114**, 1637–1672.
18 D. J. Harris and D. G. Roberts, in *The Coal Handbook: Towards Cleaner Production*, Elsevier, 2013, pp. 427–454.
19 R. J. Andrews, T. Rantell, D. Jacques, J. C. Hower, J. Steven Gardner and M. Amick, Mild coal extraction for the production of anode coke from Blue Gem coal, *Fuel*, 2010, **89**, 2640–2647.
20 C. Thompson, G. Frank, V. Edwards, M. Martinelli, A. Vego, F. Vautard, E. Cakmak, J. Craddock, M. Meier, R. Andrews and M. Weisenberger, Mesophase pitch-based high performance carbon fiber production using coal extracts from mild direct coal liquefaction, *Carbon*, 2024, **226**, 119212.
21 J.-C. Yan, Z.-Q. Bai, J. Bai and W. Li, Chemical structure and reactivity alterations of brown coals during thermal treatment with aromatic solvents, *Fuel Process. Technol.*, 2015, **137**, 117–123.
22 P. Hao, Z. Bai, R. Hou, J. Xu, J. Bai, Z. Guo, L. Kong and W. Li, Effect of solvent and atmosphere on product distribution, hydrogen consumption and coal structural change during preheating stage in direct coal liquefaction, *Fuel*, 2018, **211**, 783–788.
23 D. Fang, G. Wang, Q. Sheng, S. Ge, C. Gao and J. Gao, Preparation of hydrogen donor solvent for asphaltenes efficient liquid-phase conversion via heavy cycle oil selective hydrogenation, *Fuel*, 2019, **257**, 115886.
24 P. Hou, Y. Zhou, W. Guo, P. Ren, Q. Guo, H. Xiang, Y.-W. Li, X.-D. Wen and Y. Yang, Rational design of hydrogen-donor solvents for direct coal liquefaction, *Energy Fuels*, 2018, **32**, 4715–4723.
25 D. Zhang, C. Mu, Y. He, W. Lai, H. Liu, Q. Liu, J. Yao, X. Zhang, X. Wang, Z. Xue, Y. Nie and K. Song, Preparation and characterization of high performance coal tar pitch-based carbon fiber, *Fullerenes, Nanotubes, Carbon Nanostruct.*, 2024, **32**, 128–140.
26 J. Guo, Z. Li, B. Li, P. Chen, H. Zhu, C. Zhang, B. Sun, Z. Dong and X. Li, Hydrogenation of coal tar pitch for improved mesophase pitch molecular orientation and carbon fiber processing, *J. Anal. Appl. Pyrolysis*, 2023, **174**, 106146.
27 J. Guo, X. Li, H. Xu, H. Zhu, B. Li and A. Westwood, Molecular structure control in mesophase pitch via Co-carbonization of coal tar pitch and petroleum pitch for production of carbon fibers with both high mechanical properties and thermal conductivity, *Energy Fuels*, 2020, **34**, 6474–6482.
28 H. Shimanoe, T. Mashio, K. Nakabayashi, T. Inoue, M. Hamaguchi, J. Miyawaki, I. Mochida and S.-H. Yoon, Manufacturing spinnable mesophase pitch using direct coal extracted fraction and its derived mesophase pitch based carbon fiber, *Carbon*, 2020, **158**, 922–929.
29 J. D. Craddock, G. Frank, M. Martinelli, J. Lacy, V. Edwards, A. Vego, C. Thompson, R. Andrews and M. C. Weisenberger, Isotropic pitch-derived carbon fiber from waste coal, *Carbon*, 2024, **216**, 118590.
30 Mitsubishi, Mitsubishi pitch fiber, **https://mccfc.com/pitch-fiber/**, (accessed 22 September 2025).
31 Nippon Graphite Fiber Corporation, Technical data, **https://www.ngfworld.com/en/skill.html**, (accessed 23 September 2025).
32 Y. Zhang, G. Shu, J. Jin, M. Cui, X. Wu, X. Ren, S. Liang, J. Huang, M. Yuan, J. Gao and Y. Zhu, European Patent Office, EP1783194A1, 2007.
33 Department of Trade and Industry, *Technology status report - coal liquefaction*, London, 1999.
34 H. Ritchie, V. Samborska and R. Max, Plastic pollution, **https://ourworldindata.org/plastic-pollution?utm_source=newsletter**, (accessed 22 September 2025).

© 2026 The Author(s). Co-published by the Institute of Process Engineering, Chinese Academy of Sciences and the Royal Society of Chemistry

Open Access Article. Published on 03 October 2025. Downloaded on 5/6/2026 3:37:47 PM.
This article is licensed under a Creative Commons Attribution 3.0 Unported Licence.

35 P. G. C. Nayanathara Thathsarani Pilapitiya and A. S. Ratnayake, The world of plastic waste: A review, *Cleaner Mater.*, 2024, **11**, 100220.
36 Y. Liang, Q. Tan, Q. Song and J. Li, An analysis of the plastic waste trade and management in Asia, *Waste Manage.*, 2021, **119**, 242–253.
37 C. Jehanno, J. W. Alty, M. Roosen, S. De Meester, A. P. Dove, E. Y. X. Chen, F. A. Leibfarth and H. Sardon, Critical advances and future opportunities in upcycling commodity polymers, *Nature*, 2022, **603**, 803–814.
38 Z. Chen, W. Lu, R. Paneru, Q. Yang, W. Gong, S. Tie Tjeng, A. Goroncy, Q. Dai, J. Zhang, D. M. Kammen, T. Wang and M. Fan, Transformative and sustainable approach to waste plastic mixture valorization, *Chem. Eng. J.*, 2024, **499**, 156558.
39 M. Yang, L. Guo, G. Hu, X. Hu, J. Chen, S. Shen, W. Dai and M. Fan, Adsorption of CO_2 by Petroleum Coke Nitrogen-Doped Porous Carbons Synthesized by Combining Ammoxidation with KOH Activation, *Ind. Eng. Chem. Res.*, 2016, **55**, 757–765.
40 L. Xu, Y. Liu, Y. Li, Z. Lin, X. Ma, Y. Zhang, M. D. Argyle and M. Fan, Catalytic CH_4 reforming with CO_2 over activated carbon based catalysts, *Appl. Catal., A*, 2014, **469**, 387–397.
41 P. A. Kots, B. C. Vance, C. M. Quinn, C. Wang and D. G. Vlachos, A two-stage strategy for upcycling chlorine-contaminated plastic waste, *Nat. Sustain.*, 2023, **6**, 1258–1267.
42 B. Zhang, H. Zhang, Y. Pan, J. Shao, X. Wang, Y. Jiang, X. Xu and S. Chu, Photoelectrochemical conversion of plastic waste into high-value chemicals coupling hydrogen production, *Chem. Eng. J.*, 2023, **462**, 142247.
43 J. Zhao, J. Gao, D. Wang, Y. Chen, L. Zhang, W. Ma and S. Zhao, Microwave-intensified catalytic upcycling of plastic waste into hydrogen and carbon nanotubes over self-dispersing bimetallic catalysts, *Chem. Eng. J.*, 2024, **483**, 149270.
44 J. M. Williams, M. P. Nitzsche, L. Bromberg, Z. Qu, A. J. Moment, T. A. Hatton and A.-H. A. Park, Hybrid thermo-electrochemical conversion of plastic wastes commingled with marine biomass to value-added products using renewable energy, *Energy Environ. Sci.*, 2023, **16**, 5805–5821.
45 Y. Liu, C. Zhang, J. Feng, X. Wang, Z. Ding, L. He, Q. Zhang, J. Chen and Y. Yin, Integrated photochromic-photothermal processes for catalytic plastic upcycling, *Angew. Chem., Int. Ed.*, 2023, **62**, e202308930.
46 RecyclingMarkets.net Staff, Recycled plastic prices continue to climb higher, **https://resource-recycling.com/plastics/2024/05/15/recycled-plastic-prices-continue-to-climb-higher/**, (accessed 5 December 2024).
47 W. Ding, J. Liang and L. L. Anderson, Kinetics of thermal and catalytic coal liquefaction with plastic-derived liquids as solvent, *Ind. Eng. Chem. Res.*, 1997, **36**, 1444–1452.
48 M. M. Taghiei, Z. Feng, F. E. Huggins and G. P. Huffman, Coliquefaction of waste plastics with coal, *Energy Fuels*, 1994, **8**, 1228–1232.
49 Z. Feng, J. Zhao, J. Rockwell, D. Bailey and G. Huffman, Direct liquefaction of waste plastics and coliquefaction of coal-plastic mixtures, *Fuel Process. Technol.*, 1996, **49**, 17–30.
50 W. B. Ding, W. Tuntawiroon, J. Liang and L. L. Anderson, Depolymerization of waste plastics with coal over metal-loaded silica-alumina catalysts, *Fuel Process. Technol.*, 1996, **49**, 49–63.
51 W. Wang, A. Gallacher, K. Jolley, M. G. Nelson and E. Eddings, Harnessing high-density-polyethylene-derived liquid as a model solvent for the co-liquefaction of low-rank coals: Toward sustainable mesophase pitch for making high-quality carbon fibers from waste plastics, *Sustainability*, 2025, **17**, 4750.
52 I. Mochida, Y. Korai, C.-H. Ku, F. Watanabe and Y. Sakai, Chemistry of synthesis, structure, preparation and application of aromatic-derived mesophase pitch, *Carbon*, 2000, **38**, 305–328.
53 C. Banerjee, V. K. Chandaliya and P. S. Dash, Recent advancement in coal tar pitch-based carbon fiber precursor development and fiber manufacturing process, *J. Anal. Appl. Pyrolysis*, 2021, **158**, 105272.
54 C. Berrueco, P. Álvarez, N. Díez, M. Granda, R. Menéndez, C. Blanco, R. Santamaria and M. Millan, Characterisation and feasibility as carbon fibre precursors of isotropic pitches derived from anthracene oil, *Fuel*, 2012, **101**, 9–15.
55 J. Liu, C. Shen, L. Huang, T. Fang, Y. Li, D. Liang and Q. Xie, Preparation of pitch precursor with excellent spinnability for general-purpose carbon fibre using coal tar pitch as raw material, *Chin. J. Chem. Eng.*, 2023, **54**, 22–28.
56 W. A. Burgess and M. C. Thies, Molecular structures for the oligomeric constituents of petroleum pitch, *Carbon*, 2011, **49**, 636–651.
57 J. Liu, X. Chen, D. Liang and Q. Xie, Development of pitch-based carbon fibers: A review, *Energy Sources, Part A*, 2020, **46**, 14492–14512.
58 X. Wang, X. He and X. Wang, FTIR analysis of the functional group composition of coal tar residue extracts and extractive residues, *Appl. Sci.*, 2023, **13**, 5162.
59 Y. Zhu, Y. Xu, C. Hu, X. Yin, C. Zhao, L. Gao and X. Zhao, Preparation and characterization of mosaic coke from heavy-phase coal pitch, *Asia-Pac. J. Chem. Eng.*, 2019, **14**, e2369.
60 J. Zhang, Y. Guo, D. Pau, K. Li, K. Xie and Y. Zou, Pyrolysis kinetics and determination of organic components and N-alkanes yields of Karamay transformer oil using TG, FTIR and Py-GC/MS analyses, *Fuel*, 2021, **306**, 121691.
61 J. Drbohlav and W. T. K. Stevenson, The oxidative stabilization and carbonization of a synthetic mesophase pitch, part ii: the carbonization process, *Carbon*, 1995, **33**, 713–731.
62 J. V. Ibarra, I. Cervero and R. Moliner, Structural characterization of low temperature pyrolysis tars and their relation with parent coals, *Fuel Process. Technol.*, 1989, **22**, 135–149.
63 J. Drbohlav and W. T. K. Stevenson, The oxidative stabilization and carbonization of a synthetic mesophase

© 2026 The Author(s). Co-published by the Institute of Process Engineering, Chinese Academy of Sciences and the Royal Society of Chemistry

Open Access Article. Published on 03 October 2025. Downloaded on 5/6/2026 3:37:47 PM.
This article is licensed under a Creative Commons Attribution 3.0 Unported Licence.

pitch, part I: The oxidative stabilization process, *Carbon*, 1995, **33**, 693–711.

64 B. Smith, *Infrared spectral interpretation: A systematic approach*, CRC Press, 2018.

65 L. Shoko, J. P. Beukes and C. A. Strydom, Determining the baking isotherm temperature of Söderberg electrodes and associated structural changes, *Miner. Eng.*, 2013, **49**, 33–39.

66 F. Fanjul, M. Granda, R. Santamaría and R. Menéndez, On the chemistry of the oxidative stabilization and carbonization of carbonaceous mesophase, *Fuel*, 2002, **81**, 2061–2070.

67 G. Yuan, X. Li, X. Xiong, Z. Dong, A. Westwood, B. Li, C. Ye, G. Ma, Z. Cui, Y. Cong, J. Zhang and Y. Li, A comprehensive study on the oxidative stabilization of mesophase pitch-based tape-shaped thick fibers with oxygen, *Carbon*, 2017, **115**, 59–76.

68 T. Guan, G. Zhang, J. Zhao, J. Wang and K. Li, Insight into the oxidative reactivity of pitch fractions for predicting and optimizing the oxidation stabilization of pitch, *Fuel*, 2019, **242**, 184–194.

69 C. Q. Yang and J. R. Simms, Infrared spectroscopy studies of the petroleum pitch carbon fiber—I. The raw materials, the stabilization, and carbonization processes, *Carbon*, 1993, **31**, 451–459.

70 K. Yanagida, T. Sasaki, K. Tate, A. Sakanishi, Y. Korai and I. Mochida, Oxidation reactivity of mesophase pitch derived from C9 alkylbenzenes, *Carbon*, 1993, **31**, 577–582.

71 C. Sellitti, J. L. Koenig and H. Ishida, Surface characterization of graphitized carbon fibers by attenuated total reflection fourier transform infrared spectroscopy, *Carbon*, 1990, **28**, 221–228.

72 G. M. Pennock, G. H. Taylor and J. D. F. Gerald, Microstructure in a series of mesophase pitch-based fibers from du pont: Zones, folds, and disclinations, *Carbon*, 1993, **31**, 591–609.

73 Y. Arai, *Structure and properties of pitch-based carbon fibers*, OSTI.GOV, 1993.

74 F. Tuinstra and J. L. Koenig, Raman spectrum of graphite, *J. Chem. Phys.*, 1970, **53**, 1126–1130.

75 M. S. Dresselhaus, G. Dresselhaus, P. C. Eklund and D. D. L. Chung, Lattice vibrations in graphite and intercalation compounds of graphite, *Mater. Sci. Eng.*, 1977, **31**, 141–152.

76 Y. Kawashima and G. Katagiri, Fundamentals, overtones, and combinations in the Raman spectrum of graphite, *Phys. Rev. B: Condens. Matter Mater. Phys.*, 1995, **52**, 10053–10059.

77 D. Lu, G. Zhang, B. Li, H. Zhu, Y. Cong, Z. Dong, X. Li and J. Guo, Improving molecular stacking perfection of coal tar pitch based mesophase pitches for regulating microstructure of their carbon fibers via a low-cost co-carbonization process, *Carbon*, 2025, **238**, 120315.

78 T. Tomaru, Y. Awakura, M. Kotajima, T. Irisawa, S.-J. Ha, Y.-P. Jeon, K. Nakabayashi, J. Miyawaki and S.-H. Yoon, Effects of chemical structure of mesogenic components on the mechanical properties of mesophase pitch-based carbon fiber, *Carbon*, 2025, **242**, 120428.

79 H. Wu, G. Ye, K. Shi, D. Huang, H. Quan, C. Ye, S. Zhu, Z. Fan, F. Qian, H. Liu and J. Liu, Constructing the pyrolysis kinetic model of mesophase pitch for improving mechanical properties and thermal conductivity of carbon fibers, *Carbon*, 2025, **232**, 119765.

80 B. Niu, L. Jin, Y. Li, Z. Shi, H. Yan and H. Hu, Interaction between hydrogen-donor and nondonor solvents in direct liquefaction of bulianta coal, *Energy Fuels*, 2016, **30**, 10260–10267.

81 X. Li, S. Hu, L. Jin and H. Hu, Role of iron-based catalyst and hydrogen transfer in direct coal liquefaction, *Energy Fuels*, 2008, **22**, 1126–1129.

82 E. J. Kuhlmann, D. Y. Jung, R. P. Guptill, C. A. Dyke and H. K. Zang, Coal liquefaction using a hydrogenated creosote oil solvent, *Fuel*, 1985, **64**, 1552–1557.

83 I. Mochida and K. Sakanishi, Catalysis in coal liquefaction, *Adv. Catal.*, 1994, **40**, 39–85.

84 L. Li, Y. Hou, W. Wu, S. Liang and S. Ren, Behaviors of tetralin and 9,10-dihydroanthracene as hydrogen donor solvents in the hydrogenolysis of coal-related model compounds, *Fuel Process. Technol.*, 2019, **191**, 202–210.

85 R. Sakata, A. Takayama, K. Sakanishi and I. Mochida, Roles of nondonor solvent in the hydrogen-transferring liquefaction of Australian brown coal, *Energy Fuels*, 1990, **4**, 585–588.

86 R. Neavel, Liquefaction of coal in hydrogen-donor and non-donor vehicles, *Fuel*, 1976, **55**, 237–242.

87 I. Hakkimetecan, A. Ozkan, R. Isler, J. Yanik, M. Saglam and M. Yuksel, Naphtha derived from polyolefins, *Fuel*, 2005, **84**, 619–628.

88 W. Ding, J. Liang and L. L. Anderson, Thermal and catalytic degradation of high density polyethylene and commingled post-consumer plastic waste, *Fuel Process. Technol.*, 1997, **51**, 47–62.

89 A. Oberlin, Carbonization and graphitization, *Carbon*, 1984, **22**, 521–541.

90 T. Matsumoto and I. Mochida, A structural study on oxidative stabilization of mesophase pitch fibers derived from coal tar, *Carbon*, 1992, **30**, 1041–1046.

91 C. A. Love-Baker, T. M. Harrell, F. Vautard, J. Klett and X. Li, Analysis of the turbostratic structures in PAN-based carbon fibers with wide-angle x-ray diffraction, *Carbon*, 2024, **224**, 119037.

92 L. G. Cançado, K. Takai, T. Enoki, M. Endo, Y. A. Kim, H. Mizusaki, A. Jorio, L. N. Coelho, R. Magalhães-Paniago and M. A. Pimenta, General equation for the determination of the crystallite size La of nanographite by Raman spectroscopy, *Appl. Phys. Lett.*, 2006, **88**, 163106.

© 2026 The Author(s). Co-published by the Institute of Process Engineering, Chinese Academy of Sciences and the Royal Society of Chemistry